

## Article

# Metabolomics and Lipidomics Study Reveals Metabolic Dysregulation in Epididymal Adipose Tissue of *db/db* Mice

Yi Ru<sup>1,†</sup>, Li Xiang<sup>1,†</sup>, Qing Shen<sup>2,3</sup>, Xiuli Su<sup>1,4</sup>, Aimin Xu<sup>2,3,5,\*</sup>, and Zongwei Cai<sup>1,4,\*</sup><sup>1</sup> State Key Laboratory of Environmental and Biological Analysis, Department of Chemistry, Hong Kong Baptist University, Hong Kong SAR, China<sup>2</sup> State Key Laboratory of Pharmaceutical Biotechnology, The University of Hong Kong, Hong Kong SAR, China<sup>3</sup> Department of Medicine, The University of Hong Kong, Hong Kong SAR, China<sup>4</sup> College of Science, Eastern Institute of Technology, Ningbo 315100, China<sup>5</sup> Department of Pharmacology & Pharmacy, The University of Hong Kong, Hong Kong SAR, China

\* Correspondence: amxu@hku.hk (A.X.); zwcai@hkbu.edu.hk (Z.C.); Tel.: +852-3917-9754 (A.X.); +852-3411-7070 (Z.C.); Fax: +852-2816-2095 (A.X.)

† These authors contributed equally to this work.

‡ These authors contributed equally to this work.

Received: 15 February 2025; Revised: 20 March 2025; Accepted: 14 May 2025; Published: 3 July 2025

**Abstract:** Type 2 diabetes (T2D) is a common chronic metabolic disease that poses a major challenge to global public health. Dysfunction of epididymal adipose tissue (eWAT) plays a pivotal role in the progression of T2D. However, the metabolic alterations occurring in eWAT under diabetic conditions remain incompletely understood. This study aims to comprehensively explore the metabolic changes in eWAT of *db/db* mice, a well-established model of T2D, by integrating untargeted metabolomics, targeted metabolomics, and lipidomics analysis. Our results reveal significant perturbations in the purine and histidine metabolic pathways. Specifically, we observed marked reductions in key metabolites, including adenosine monophosphate (AMP), xanthine, hypoxanthine, adenosine, and inosine, in the eWAT of *db/db* mice. Additionally, there were significant increases in short- and medium-chain acylcarnitines, along with elevated levels of short-chain fatty acids and tricarboxylic acid (TCA) cycle intermediates. Notably, distinct patterns of alterations in triglycerides, ceramides, and phosphatidylcholines were observed with each characterized by specific structural attributes. These results offer new perspectives on the metabolic reprogramming of eWAT in the diabetic state and identify potential targets for the development of therapeutic strategies.

**Keywords:** metabolomics; lipidomics; UHPLC-MS; type 2 diabetes; epididymal adipose tissue

## 1. Introduction

Type 2 diabetes (T2D) is a globally prevailing metabolic disorder that poses substantial public health challenges owing to its link with severe complications, including diabetic nephropathy, cardiovascular diseases, and retinopathy [1]. Insulin resistance, a metabolic condition characterized by impaired cellular sensitivity to insulin, represents a central pathophysiological feature of T2D, predominantly disrupting the functions of adipose tissue, liver, and skeletal muscle [2]. Adipose tissue is essential for maintaining systemic glucose homeostasis, functioning by sequestering surplus energy stored as triglycerides and mobilizing fatty acids during fasting states [3]. Dysregulated adipose tissue function in T2D disrupts systemic glucose and lipid metabolism, contributing to disease progression [4].

Epididymal adipose tissue (eWAT) is a distinct type of white adipose tissue marked by larger internal adipocytes and the secretion of various bioactive adipokines and inflammatory factors, which are critical for maintaining metabolic homeostasis [5]. For instance, FGF21 promotes lipid and glucose homeostasis and exhibits anti-inflammatory effects [6]. Additionally, TNF- $\alpha$  concentration is linked to the extent of IRS-1 inactivation in obese patients, which inhibits insulin receptor kinase activity, impairs GLUT-4 translocation, and ultimately reduces glucose uptake [7]. Examining the metabolic alterations in eWAT linked to T2D can aid in identifying potential diagnostic biomarkers, uncover the mechanisms driving insulin resistance, and support the development of targeted therapies to mitigate disease progression [8].



High-performance liquid chromatography-mass spectrometry (HPLC-MS) based metabolomics technology has been extensively employed to analyze small molecules across various biological matrices, providing comprehensive insights into intracellular metabolic phenotypes [9]. Non-targeted metabolomics endeavors to comprehensively profile a wide spectrum of metabolites within a biological system, enabling the discovery of novel pathophysiological pathways and potential biomarkers [10]. In contrast, targeted metabolomics emphasizes the quantitative analysis of predefined metabolites within specific metabolic pathways or structurally related groups, offering higher sensitivity and accuracy [11]. Previous studies have utilized untargeted metabolomics or lipidomics analysis to investigate the metabolic profiles of serum, urine, and major metabolic organs in various mouse models, including *ob/ob*, *db/db*, and high-fat diet and streptozotocin (HFD-STZ)-induced diabetic mice. These studies have identified notable alterations in key metabolites, including lysine, branched-chain amino acids, fatty acids, acylcarnitines, and acylglycines [12–15]. However, comprehensive analyses of the metabolic landscape in eWAT under diabetic conditions are still scarce. Moreover, the integration of untargeted and targeted metabolomics analysis combines sensitivity and specificity, facilitating the identification of a broader range of metabolites or metabolic networks [16]. For instance, Zhang et al. detected 16 distinct serum biomarkers for lung cancer using untargeted methods and 9 additional biomarkers through targeted approaches, significantly enhancing the overall identification of biomarkers [17]. Furthermore, Wang et al. and Chen et al. emphasized that relying solely on either metabolomics or lipidomics is inadequate to fully capture the complexity of metabolic disturbances [18,19]. Thus, the integration of metabolomics and lipidomics is essential for a holistic understanding of metabolic alterations in eWAT under T2D conditions and for identifying potential therapeutic targets.

In this study, we utilized *db/db* mice as a model for T2D and employed an integrated approach that combined untargeted metabolomics, targeted metabolomics, and lipidomics to systematically characterize the metabolic landscape of eWAT. This study aims to identify key metabolic pathways disrupted under diabetic conditions, providing a deeper understanding of eWAT metabolism in T2D. These results could aid in identifying new biomarkers or therapeutic targets for diabetes regulation.

## 2. Materials and Methods

### 2.1. Materials

3-Nitrophenylhydrazine hydrochloride (3-NPH), pyridine, and various certified standard compounds were procured from reputable suppliers such as Sigma-Aldrich (St. Louis, MO, USA) and Cambridge Isotope Laboratories (CIL, Andover, MA, USA). 1-Ethyl-3-(3-dimethylaminopropyl)carbodiimide hydrochloride (EDCI, purity  $\geq 98\%$ ) was sourced from Tokyo Chemical Industry (TCI, Japan). High-performance liquid chromatography (HPLC)-grade methanol, acetonitrile and methyl tert-butyl ether (MTBE) were purchased from RIC Labscan Ltd. (Bangkok, Thailand). Unless otherwise indicated, all additional chemicals and solutions used were of analytical grade.

### 2.2. Animal Experiments

Male C57BL/KsJ *db/db* mice and their *db/m*+ littermates, aged 12 weeks, were selected for experiments. The mice were sourced from the Animal Facility of The Chinese University of Hong Kong (CUHK). All animal experimental procedures were approved by the Hong Kong Government and Department of Health. The mice were kept in the environment with maintained humidity and temperature, under a 12-h light/dark cycle. They were given standard laboratory food ad libitum and had free access to water.

We monitored body weight, fasting blood glucose, and insulin levels. Following euthanasia by CO<sub>2</sub> inhalation, blood samples were obtained from the inferior vena cava and transferred into centrifuge tubes containing pre-wetted sodium heparin. eWAT was collected and kept under  $-80\text{ }^{\circ}\text{C}$  until further analysis.

### 2.3. Sample Preparation

For metabolomics analysis, 30 mg of eWAT was weighed into a centrifuge tube. Thereafter, 800  $\mu\text{L}$  of ice-cold 80% methanol/water solution (80/20, v/v) containing internal standards (IS) was added for homogenization using a homogenizer (Wuhan Servicebio Technology Co., Ltd., Wuhan, China). The samples were then sonicated for 10 min and incubated at 4  $^{\circ}\text{C}$  for 15 min. Then the samples were centrifuged at 14,200 $\times g$  for 15 min. The supernatant was dried and reconstituted in 50% methanol/water for analysis.

For lipidomics analysis, 20 mg of eWAT was combined with 170  $\mu\text{L}$  of water and 480  $\mu\text{L}$  of MTBE/methanol mixture (5:1, v/v). The mixture was homogenized for 10 min at 4  $^{\circ}\text{C}$  and then centrifuged at 3000 rpm for 10 min at 4  $^{\circ}\text{C}$ . A 300  $\mu\text{L}$  aliquot of the supernatant was evaporated to dryness under vacuum at 4  $^{\circ}\text{C}$ . The dried samples

were reconstituted in 60  $\mu$ L of dichloromethane/methanol mixture (1:1, v/v) containing internal standards for lipidomics analysis.

For both non-targeted metabolomics and lipidomics analyses, quality control (QC) samples were generated by mixing supernatant extracts from individual samples. These QC samples were injected throughout the experiment to evaluate instrument stability and reliability. Authentic standards were used for all targeted compounds, with stock solutions prepared in 50% methanol and subsequently diluted to appropriate concentrations for method development and validation.

#### 2.4. H&E Staining

The experimental procedure was adapted with minor adjustments from the protocol described by Jin et al. [20]. The eWAT samples were fixed in 10% formalin for 72 h. After fixation, the tissues were dehydrated, embedded in paraffin, and sectioned. The sections were incubated at 65 °C for 20 min, followed by deparaffinization and rehydration. Thereafter, the sections were stained according to the standard hematoxylin and eosin (H&E) protocol.

#### 2.5. UHPLC-MS/MS Analysis

Untargeted metabolomics, lipidomics, and acylcarnitine analyses were performed using an ultra-high-performance liquid chromatography system coupled with a Q Exactive Focus Orbitrap mass spectrometer (Thermo Fisher Scientific, Waltham, MA, USA). This procedure was partially modified from the method reported by Xiang et al. [9]. For the relative quantification of fatty acids and intermediates of the tricarboxylic acid (TCA) cycle, a 3NPH-based derivatization method was employed using the UltiMate 3000 liquid chromatography tandem triple quadrupole mass spectrometer system (Thermo Fisher Scientific, Waltham, MA, USA), with modifications according to the methods described by Xiang et al. [13,21] and Jia et al. [22]. The specific chromatographic conditions and mass spectrometer parameters are presented in Tables S1–S4.

#### 2.6. Data Processing and Statistical Analysis

The data processing for targeted analysis was carried out using Xcalibur Software v.4.1 (Thermo). For non-targeted metabolomics and lipidomics analysis, chromatographic peak extraction and alignment were performed using R v4.3.0 and LipidSearch™ 5.0 Software.. To mitigate systematic errors, features with a coefficient of variation (CV) exceeding 30% in QC samples were removed. After normalization and Pareto scaling, multivariate analyses such as unsupervised Principal Component Analysis (PCA) was performed. Differential metabolites between two groups were identified based on *p* values ( $p < 0.05$ ) and fold changes ( $FC > 1.2$  or  $FC < 0.8$ ). Metabolites were identified by matching MS/MS fragments with publicly available databases, including the Human Metabolome Database (HMDB) and METLIN. Lipid identification was performed using LipidSearch software. LipidSearch incorporated retention time filtering ( $\pm 0.5$  min) to exclude lipids with retention times outside the expected ranges. Only lipids identified with confidence levels A and B, as defined by MS/MS fragment ion matching criteria, were included in the final analysis. The pathway enrichment analysis was performed utilizing the Kyoto Encyclopedia of Genes and Genomes (KEGG) database. Data are shown as mean  $\pm$  standard error (SE), with *p* values  $< 0.05$  considered statistically significant.

### 3. Results

#### 3.1. Phenotypic Characterization of eWAT in *db/m+* and *db/db* Mice

In this study, *db/db* mice were employed as a model for type 2 diabetes. Compared to the control group, *db/db* mice exhibited significantly increased blood glucose and insulin levels (Figure S1A,B), indicating severe systemic glucose metabolism dysregulation. Additionally, Figure S1C–E demonstrate that *db/db* mice had significantly higher body weight, eWAT weight, and eWAT-to-body-weight (EW/BW) ratio than the control group. These findings reflect not only substantial weight gain but also abnormal changes in eWAT under conditions of metabolic disorder. Histological analysis further revealed a marked increase in lipid droplet size within the eWAT of *db/db* mice (Figure S1F,G). These alterations suggest substantial pathological changes in the eWAT of *db/db* mice under diabetic conditions, potentially closely associated with metabolic dysregulation.

#### 3.2. Metabolic Profiles of eWAT in *db/db* Mice

Non-targeted metabolomics was employed to characterize the metabolic differences between the eWAT of *db/m+* and *db/db* mice. To assess the performance of the analytical method, we first performed PCA on both

experimental and QC samples. As shown in Figure S2A, the QC samples clustered closely together, demonstrating the stability and repeatability of the analytical method and instrument. Additionally, the PCA results, presented in Figure 1A, revealed a clear separation between the metabolic profiles of the *db/db* group and the *db/m+* group, highlighting distinct metabolic differences between these two groups.

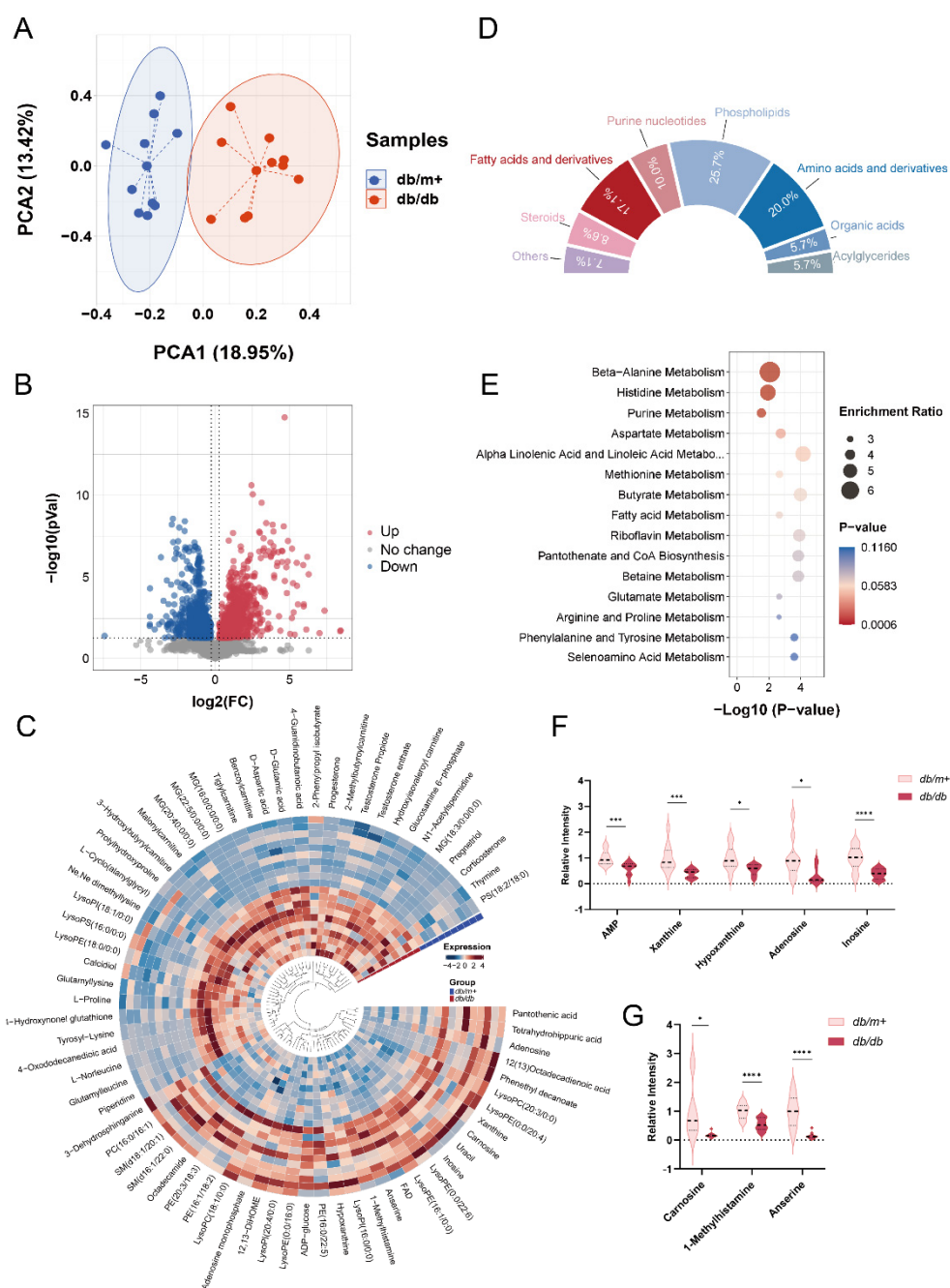


**Figure 1.** Non-targeted metabolomics analysis of eWAT in *db/db* mice. (A) PCA score plot. The enclosed area represents samples within the 95% confidence interval. (B) Volcano plot of detected features. (C) Classification summary of differential metabolites. (D) Heatmap visualization of all differential metabolites. (E) Bubble chart showing KEGG pathway enrichment analysis results based on differential metabolites. (F,G) Changes in metabolites related to purine metabolism (F) and histidine metabolism (G) in the eWAT of *db/db* mice. Data are presented as means  $\pm$  SEM (n = 10). The p value was calculated by t-student. \*  $p < 0.05$ , \*\*\*  $p < 0.005$ , \*\*\*\*  $p < 0.001$ .

### 3.3. Differential Metabolites Identification and Metabolic Pathway Enrichment

In this study, features with fold changes greater than 1.2 or less than 0.8 and p values less than 0.05 were identified as differential metabolites. The volcano plot results revealed a total of 1492 differential features, including 798 significantly upregulated and 694 significantly downregulated (Figure 1B). Among these, 70

differential features were further identified as endogenous metabolites, which are summarized in Table S5 and displayed in Figure 1C. The composition of these metabolites is shown in Figure 1D, where phospholipids, amino acids and their derivatives, and fatty acids and their derivatives represent the largest proportions, accounting for 25.70%, 20.00%, and 17.10%, respectively. This suggests that metabolic abnormalities in eWAT under diabetic conditions are predominantly reflected in lipid metabolism and certain amino acid metabolic pathways, which may potentially lead to adipose tissue dysfunction.

To further explore the metabolic pathways underlying eWAT metabolic dysregulation in *db/db* mice, pathway enrichment analysis was conducted based on the KEGG database. The results (Figure 1E) showed that histidine metabolism, alanine metabolism, and purine metabolism pathways were the most significantly altered ( $p < 0.05$ ). Specifically, adenosine monophosphate (AMP), xanthine, hypoxanthine, adenosine, and inosine in the purine metabolism pathway were markedly reduced in the eWAT of *db/db* mice (Figure 1F). Additionally, 1-methylhistamine, carnosine, and anserine, involved in histidine metabolism, exhibited a significant decrease compared to the control group (Figure 1G). The abnormal expression of these metabolic pathways may be closely associated with the metabolic dysfunction in the eWAT of *db/db* mice.

### 3.4. Targeted Metabolomics Analysis of eWAT in *db/db* Mice

Untargeted metabolomics revealed that fatty acids and their derivatives accounted for approximately 20% of the total differential metabolites, suggesting significant abnormalities in fatty acid metabolic pathways. To gain deeper insights, we conducted targeted measurements of fatty acid metabolism-related compounds in the eWAT of *db/db* mice, including various fatty acids, acylcarnitines, and TCA cycle intermediates (Tables S6 and S7).

The PCA score plot (Figure 2A) demonstrated a clear separation of the targeted metabolic profiles between the two groups, indicating significant disruption of fatty acid metabolism in the eWAT of diabetic mice. The volcano plot (Figure 2B) demonstrated that 17 metabolites were significantly upregulated, while 6 were significantly downregulated.

Interestingly, acylcarnitines with different carbon chain lengths showed distinct changes. Several butyrylcarnitine derivatives (e.g., crotonyl-carnitine (C4:1-CN), hydroxybutyrylcarnitine (C4-OH-CN), 2-methylbutyrylcarnitine (2-Me-C4-CN)), valerylcarnitine derivatives (e.g., valeryl-carnitine (C5-CN), tiglylcarnitine (C5:1-CN), hydroxyl valeryl-carnitine (C5-OH-CN), and hydroxyisovaleryl carnitine (isoC5-OH-CN)) were markedly elevated in the eWAT of *db/db* mice (Figure 2C). Additionally, several medium-chain acylcarnitines, including hydroxyl hexanoyl-carnitine (C6-OH-CN), octenoyl-carnitine (C8:1-CN), hydroxyl octanoyl-carnitine (C8-OH-CN), and decenoyl-carnitine (C10:1-CN), were significantly elevated in the *db/db* group (Figure 2D). In contrast, long-chain acylcarnitines showed no significant overall changes except for the notable increases in linoleoyl-carnitine (C18:2-CN) and hydroxyl linoleoyl-carnitine (C18:2-OH-CN) (Figure S3A). Additionally, alterations in short-chain fatty acids are depicted in Figure 2E, with 2-hydroxybutyric acid (2-OH-C4), 3-hydroxyisobutyric acid (3-OH-isoC4), and 5-hydroxyvaleric acid (5-OH-C5) significantly increased in the disease group, while propanoic acid (C3) showed a significant decrease. For the majority of medium-chain and long-chain fatty acids (Figure S3B), no significant trends were observed in the model group, except for myristic acid (C14), palmitic acid (C16), and arachidic acid (C20), which were significantly decreased in the eWAT of *db/db* mice. The TCA cycle, essential for cellular energy metabolism, was also analyzed. Targeted measurements indicated that succinate, fumarate, citrate, isocitrate, and  $\alpha$ -ketoglutarate were significantly elevated in the eWAT of diabetic mice. The above findings highlight significant disruptions in fatty acid and energy metabolism pathways in the eWAT of diabetic mice.

### 3.5. Diverse Lipid Alterations in eWAT of *db/db* Mice

Furthermore, the results showed that phospholipids constituted 25.7% of the differential metabolites, highlighting notable disruptions in lipid metabolism. Considering the pivotal role of lipids in various metabolic pathways and the substantial alterations observed in this study, we performed lipidomics analysis on eWAT to gain a deeper understanding of these lipid metabolic disturbances. The PCA plot (Figure S2B) demonstrated tight clustering of QC samples, highlighting the robustness, stability, and reproducibility of the analytical method and instrumentation. Furthermore, the PCA results (Figure 3A) revealed significant differences in eWAT lipid profiles between the two groups, indicating clear metabolic distinctions. Differential analysis identified 210 lipid species with substantial changes, including triglycerides (TG, 7.4%), diglycerides (DG, 6.0%), phosphatidylcholines (PC, 24.7%), phosphatidylethanolamines (PE, 18.6%), ceramides (Cer, 10.2%), sphingomyelins (SM, 14.0%), and hexosylceramides (Hex1Cer, 8.8%). Lipids with no significant change were excluded from further analysis (Figure 3B and Table S8).

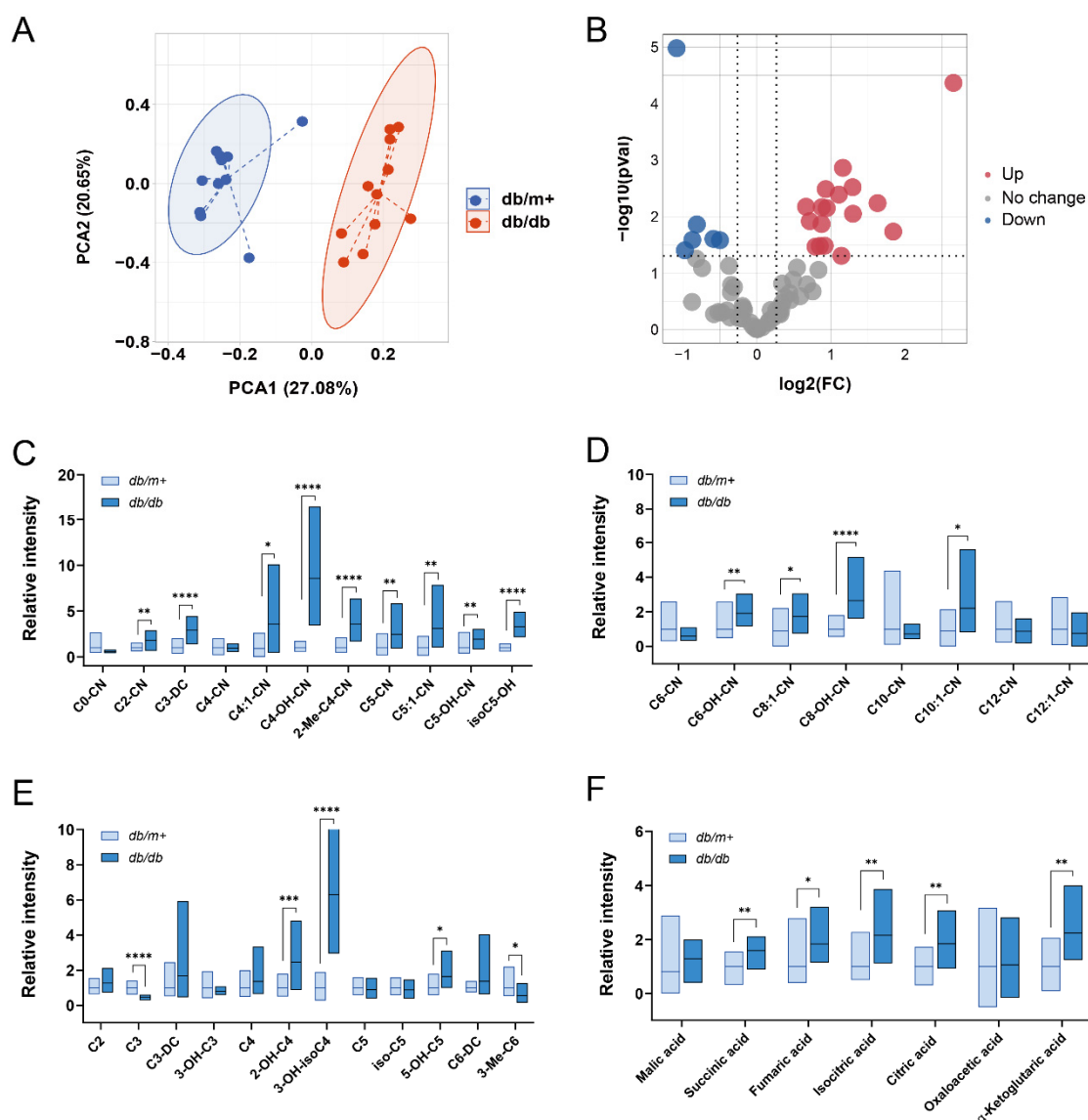


**Figure 2.** Targeted metabolomics analysis of eWAT in *db/db* mice. **(A)** PCA score plot. The enclosed area represents samples within the 95% confidence interval. **(B)** Volcano plot of differential metabolites. **(C,D)** Changes in short-chain **(C)** and medium-chain acylcarnitines. **(D)** based on integrated non-targeted and targeted metabolomics analysis. **(E,F)** Changes in short-chain fatty acids **(E)** and TCA cycle products **(F)** in the eWAT of *db/db* mice. Data are presented as means  $\pm$  SEM (n = 10). The *p* value was calculated by t-student. \* *p* < 0.05, \*\* *p* < 0.01, \*\*\* *p* < 0.005, \*\*\*\* *p* < 0.001.

To further investigate the alterations of individual lipid species under diabetic conditions, we visualized all significantly altered lipids using the bubble chart and bar graphs. Within the glycerophospholipids (Figure 3C,F), phosphatidylinositol (PI), phosphatidylserine (PS), and phosphatidylglycerol (PG) were significantly increased, while PE levels were significantly reduced in the diabetic group. Among the sphingolipids (Figure 3D,F), SM were elevated, while Hex1Cer levels were significantly decreased. Cer species showed a mixed pattern, with some species significantly increased and others significantly decreased (Figure 3F). Compared to the *db/m+* group, glycerolipids, specifically TG and DG, were significantly elevated in the diabetic group (Figure 3E,F). These findings reveal that lipid metabolism disturbances in the eWAT of *db/db* mice are widespread, affecting not only phospholipids but also glycerolipids and sphingolipids. This comprehensive analysis highlights the complex nature of diabetic lipid dysregulation and pinpoints specific lipid species that may be critical to diabetes pathophysiology.

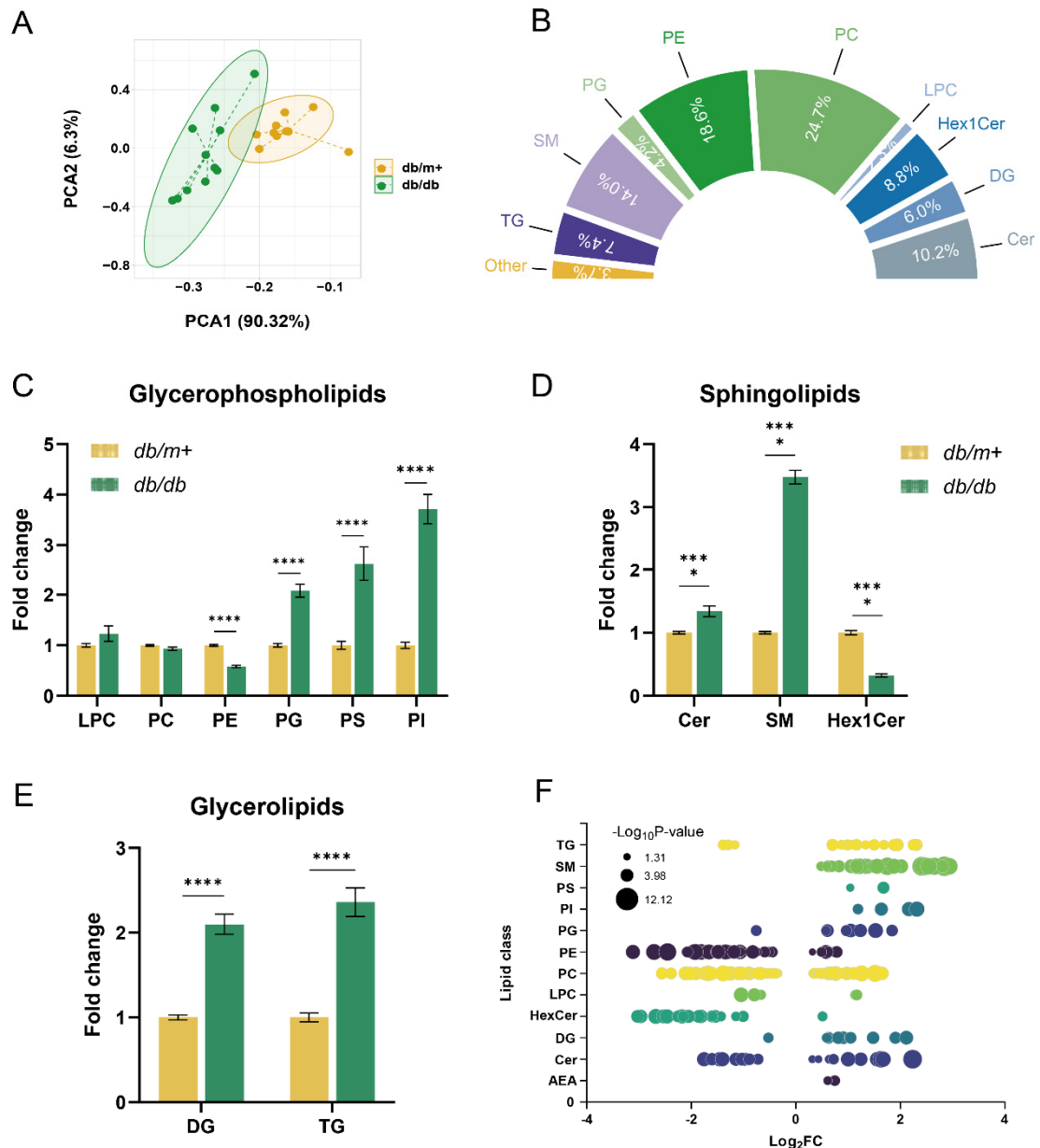


**Figure 3.** Lipidomics analysis of eWAT in *db/db* mice. (A) PCA score plot. The enclosed area represents samples within the 95% confidence interval. (B) Summary of classifications for differential lipids. (C,E) Fold changes in the intensities of (C) glycerophospholipids, (D) sphingolipids, and (E) glycerolipids. (F) Log<sub>2</sub> fold changes and significance of lipid species from different lipid categories. Each dot represents a lipid species, with the size of the dot indicating the magnitude of significance. Only lipids with  $p < 0.05$  are shown. Data are presented as means  $\pm$  SEM ( $n = 10$ ). The  $p$  value was calculated by t-student. \*\*\*\*  $p < 0.001$ .

### 3.6. Structural Alterations of Lipids in eWAT of diabetic Mice

To elucidate the structural alterations of differential lipids in eWAT under diabetic conditions, we analyzed variations in carbon chain length, degree of unsaturation, and acyl side chains of different lipid molecules. TG with carbon chain length ranging from 42 to 50 and double bond counts between 0 and 3 exhibited a notable increase in eWAT of *db/db* mice (Figure 4A). Similarly, DG with total carbon numbers ranging from 26 to 36 and double bond numbers between 1 and 4 exhibited substantial changes, whereas DGs with carbon numbers greater than 39 exhibited minor alterations (Figure 4B).

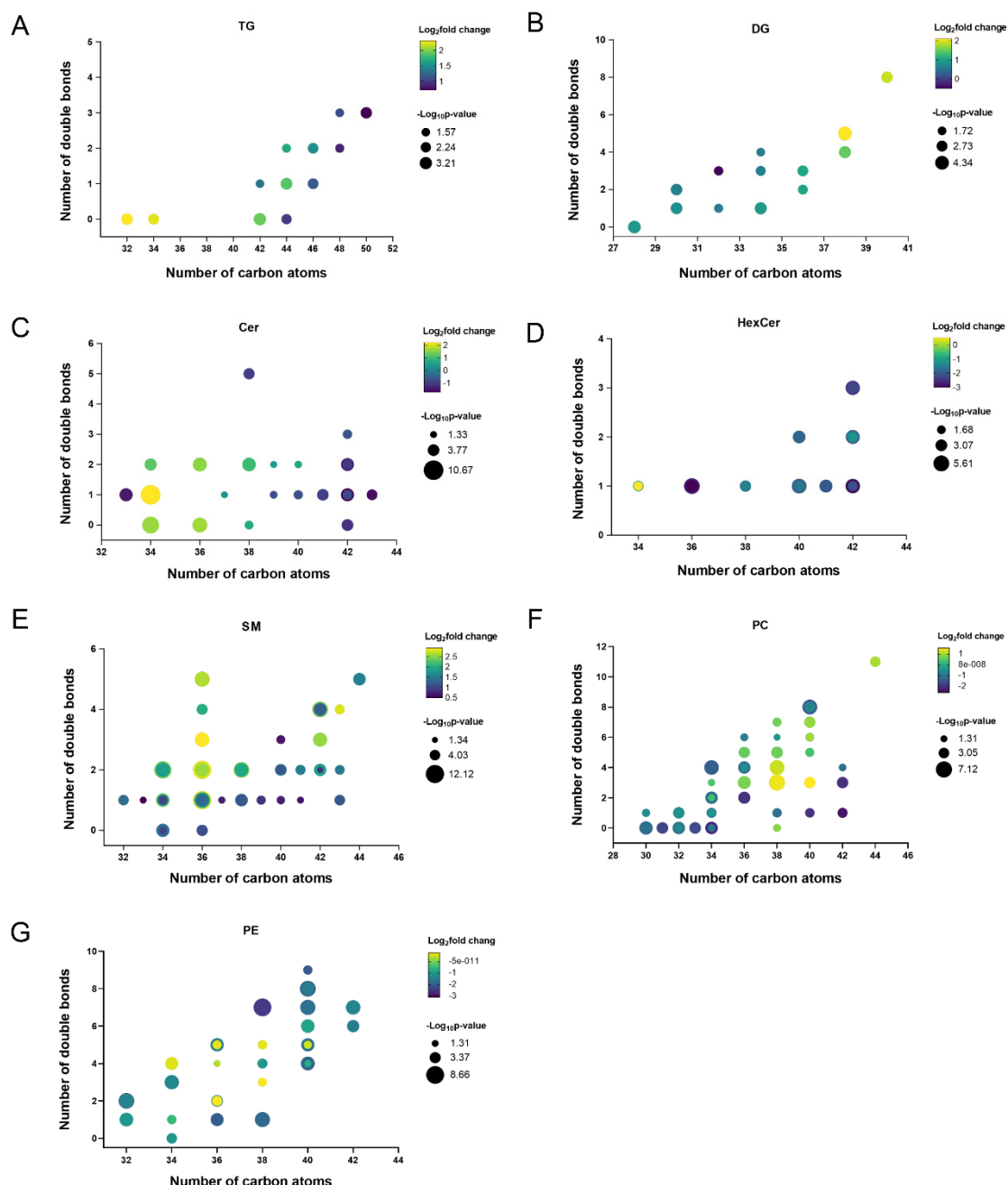


**Figure 4.** Bubble plot analysis of different categories of lipid molecular structures in the eWAT of *db/db* mice (A–G). Structural information of (A) triglycerides, (B) diglycerides, (C) ceramides, (D) hexosylceramides, (E) sphingomyelins, (F) phosphatidylcholines, and (G) phosphatidylethanolamines. The size of each bubble represents the magnitude of significance, while different colors indicate varying fold changes. The *p* value was calculated by t-student.

In the sphingolipid category, the most significantly altered ceramides had unsaturation levels below 2. Cer molecules with carbon numbers between 31 and 38 showed a significant increase, while those between 39 and 43 showed a significant decrease in the disease group (Figure 4C). Moreover, most of Cer molecules containing C18:1 acyl side chain was markedly reduced (Figure S4A). Hex1Cer levels overall decreased, with notable changes in molecules with carbon numbers between 40–42 (Figure 4D). Sphingomyelins (SM) exhibited a significant upward trend, particularly those with total carbon numbers between 34 and 38 and double bond counts greater than 2 (Figure 4E).

Phospholipids in eWAT also showed distinct alteration patterns. Phosphatidylcholines (PC) with carbon numbers between 36 and 40 and double bond counts between 3 and 7 were significantly elevated, while PCs with fewer than 36 carbons decreased significantly (Figure 4F). Most phosphatidylethanolamine (PE) molecules were

significantly reduced in eWAT of diabetic mice (Figure 4G), although PE molecules with acyl side chains containing 20:4 and 20:3 accumulated substantially in eWAT of diabetic mice (Figure S4B).

These findings suggest that lipid metabolism in eWAT undergoes extensive reprogramming under T2D conditions, characterized by significant alterations in the carbon chain length, degree of unsaturation, and acyl side chains of various lipid species.

#### 4. Discussion

Type 2 diabetes is a globally prevalent metabolic disorder, yet the comprehensive metabolic profile of eWAT under diabetic conditions remains incompletely understood. To address this knowledge gap, we employed a complementary strategy integrating untargeted metabolomics, targeted metabolomics, and lipidomics to analyze the eWAT of *db/db* diabetic mice. This integrative approach significantly enhanced the detection coverage, sensitivity, and accuracy of metabolite profiling. The Figure 5 presents a proposed metabolic overview of the eWAT in *db/db* mice, highlighting disrupted metabolic pathways and altered metabolites. Specifically, disruptions in the TCA cycle, purine metabolism, histidine metabolism, and lipid metabolism, including changes in glycerolipids, glycerophospholipids, sphingolipids, short- and medium-chain acylcarnitines, and short-chain fatty acids, shed light on the complex mechanisms underlying T2D.

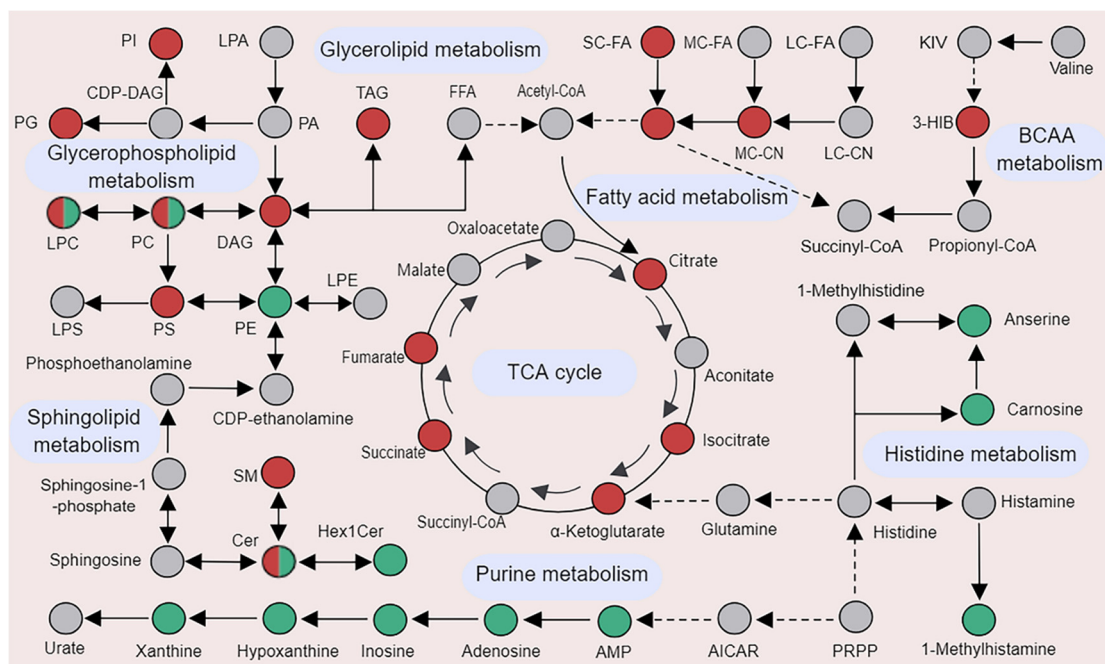


**Figure 5.** An overview of disrupted metabolic pathways in the eWAT of *db/db* mice. Red, green, and gray colors indicate increased, decreased, and unchanged levels in *db/db* mice, respectively.

Several studies have demonstrated a close association between the purine metabolism and T2D [23,24]. Elevated levels of purine metabolism intermediates, such as adenosine, xanthine, hypoxanthine, and AMP, have been reported in the serum of T2D patients and animal models [25,26]. However, our findings revealed a significant reduction in intermediates such as adenosine, AMP, inosine, hypoxanthine, and xanthine in the eWAT of diabetic mice. This observation partially aligns with prior studies reporting decreased adenosine and inosine levels in the eWAT of *db/db* and *ob/ob* mice [12]. These tissue-specific alterations may reflect distinct metabolic adaptations in eWAT under diabetic conditions. Adenosine holds a critical role in adipose tissue by inhibiting lipolysis and enhancing insulin-stimulated glucose uptake. Therefore, its reduction may exacerbate fat accumulation and insulin resistance, further disrupting glucose metabolism [27]. Similarly, reductions in xanthine and hypoxanthine, which are involved in oxidative stress responses, may impair antioxidant defenses, leading to increased oxidative damage and contributing to the progression of T2D [28,29]. Additionally, inosine, which is essential for anti-inflammatory and antioxidant responses, may also have significant implications. Its reduction could amplify inflammatory responses and metabolic dysfunction, potentially contributing to the chronic inflammation commonly observed in diabetic conditions [30]. These findings suggest that purine metabolism disturbances in eWAT are tightly linked to T2D pathology.

Furthermore, we observed notable disruptions in histidine metabolism, evidenced by the notable reduction in 1-methylhistidine, carnosine, and anserine levels in eWAT. Previous studies also reported reduced muscle carnosine or anserine content in T2D patients [31] and the kidney of *db/db* mice [32], suggesting that these changes are common across multiple tissues. The decreased levels of 1-methylhistamine indicate abnormalities in histidine metabolism and potential histamine accumulation, both of which are associated with increased fasting blood glucose (FBG) [33], insulin resistance, and reduced insulin sensitivity [34]. As antioxidants and antiglycation agents, carnosine and anserine play a protective role against oxidative stress and cellular damage [35]. Their reduction in eWAT could exacerbate diabetic complications by increasing oxidative stress and inflammation [36]. While the precise role of these disruptions remains unclear, they may represent adaptive or pathological responses to the diabetic state. Further functional studies are needed to explore the mechanistic implications of these alterations, which could provide insights into the metabolic dysregulation in eWAT and identify potential therapeutic targets for type 2 diabetes.

In our study, a notable increase in 3-hydroxyisobutyrate (3HIB), a catabolic intermediate of valine, was observed in diabetic mice. This finding aligns with previous studies that reported elevated circulating 3-HIB levels in large-scale cohorts of T2D patients [37]. In addition, treatment with 3-HIB has been shown to enhance fatty acid uptake, modulate glucose uptake in response to insulin, and reduce mitochondrial oxygen consumption and reactive oxygen species in white adipocytes [38]. Moreover, most short- and medium-chain acylcarnitines were significantly elevated in the eWAT of diabetic mice, whereas long-chain acylcarnitines showed no substantial changes. This pattern suggests an impairment of the fatty acid  $\beta$ -oxidation process, resulting in the accumulation of these intermediates and preventing their further metabolism [39]. Similar elevations in acylcarnitines have been observed in the adipose tissue of NZO mice, an obese diabetic mouse model [40]. Additionally, increasing levels of medium-chain acylcarnitines are linked to gestational diabetes, potentially impeding insulin production in response to glucose stimulation [41]. These observations indicate that disruptions in fatty acid metabolism within adipose tissues may result in the accumulation of short- and medium-chain acylcarnitines, subsequently raising their circulating levels and exacerbating diabetes and its complications.

Moreover, most TCA cycle intermediates were markedly elevated in the eWAT of diabetic mice. This observation aligns with previous findings reporting increased levels of these metabolites in subcutaneous white adipose tissue of T2D patients [8] and the urine of *db/db* mice [42]. The elevation of TCA cycle intermediates may reflect a compensatory increase in TCA cycle activity due to disturbances in energy metabolism, yet it might also lead to mitochondrial dysfunction and tissue insulin resistance [43]. The hyperactivation of the TCA cycle may result in the accumulation of its intermediates, obstructing the entry of fatty acid  $\beta$ -oxidation intermediates into the TCA cycle, thereby worsening the accumulation of short- and medium-chain acylcarnitines and causing an imbalance in energy metabolism [44].

Lipidomics analysis exhibited a significant increase in TG and DG in eWAT of *db/db* mice. Notably, TG species with total carbon numbers ranging from 42 to 50 and containing 0 to 3 double bonds were markedly elevated. This pattern reflects a shift toward the synthesis and storage of longer-chain fatty acids with lower degrees of unsaturation under diabetic conditions. Our findings are consistent with previous studies that identified a strong association between TG species with 48–50 carbon atoms and 2–3 double bonds and the development of T2D [45]. These results indicate that TG molecules with specific structural characteristics may contribute to the pathogenesis of T2D. Furthermore, ceramide accumulation in major metabolic tissues is a well-established contributor to decreased insulin sensitivity during diabetes [46]. In the eWAT of *db/db* mice, we observed a significant increase in ceramides with total carbon numbers ranging from 31 to 38, primarily containing C16 and C18 acyl chains, while ceramides with total carbon numbers between 39 and 43, containing C20 to C24 acyl chains, were significantly reduced. This shift in ceramide profiles likely reflects alterations in ceramide synthesis pathways under diabetic conditions. Ceramides with C16 and C18 acyl chains are synthesized by CerS1, CerS5, and CerS6, whereas CerS2 mediates the synthesis of ceramides containing very long-chain acyl groups [46]. Modulating CerS6 expression has been reported to reduce C16:0 ceramide levels and improve insulin resistance [47], while overexpressing CerS2 in the liver increases very long-chain ceramides and enhances insulin sensitivity [48]. These findings suggest that different ceramide species may have distinct impacts on glucose homeostasis, and the protective role of specific long-chain ceramides in diabetes warrants further investigation. Hexosylceramides, which consist of a hydrophilic hexose (glucose or galactose) linked to a hydrophobic ceramide backbone, were found to be reduced in the eWAT of *db/db* mice. Notably, lower levels of lactosylceramide and hexosylceramide have been positively associated with a higher risk of diabetic nephropathy [49] and the development of CVD in diabetic patients [50]. These findings suggest that reductions in these glycosphingolipids may contribute to the progression of diabetes-related complications. In contrast, SM levels were markedly elevated in the eWAT of diabetic mice, consistent with previous findings reporting elevated SM levels in diabetes [51]. Elevated circulating

levels of palmitoyl-sphingomyelin (PSM) are linked to a higher risk of CVD in patients with diabetes [52]. However, the precise mechanisms by which these changes in glycosphingolipid and sphingomyelin metabolism contribute to diabetes-associated pathologies remain unclear and require further investigation.

Under diabetic conditions, phospholipids in the eWAT exhibit distinct alterations. Specifically, PC with total carbon numbers ranging from 36 to 40 and containing 3 to 7 double bonds are significantly elevated, while PC species with shorter or longer carbon chains tend to decrease. This pattern of discordant changes aligns with findings from Shao et al. [53] and Yang et al. [54], who found similar changes in patients with T2D. Despite these observations, the precise role of specific PC species in the pathogenesis of T2D remains to be elucidated through further functional studies. Moreover, PE in the adipose tissue of diabetic mice is significantly reduced, mirroring similar reductions observed in the livers of type 2 diabetic mice. This decrease in PE levels may be linked to the downregulation of phosphoethanolamine cytidyltransferase (Pcyt2), a crucial enzyme involved in the de novo synthesis of PE [55]. The downregulation of Pcyt2 and the consequent decline in PE levels could contribute to the metabolic disturbances associated with diabetes.

## 5. Conclusions

In this study, we employed an integrative metabolomics and lipidomics approach to elucidate the metabolic alterations in eWAT of *db/db* mice. Our comprehensive analysis revealed significant and distinctive changes in acylglycerides, sphingolipids, and phospholipids, as well as disruptions in histidine and purine metabolism. Furthermore, targeted metabolomics demonstrated pronounced disturbances in fatty acid oxidation and energy metabolism, as evidenced by the upregulation of various acylcarnitine derivatives and TCA cycle intermediates. These findings underscore the profound metabolic changes in eWAT associated with T2D, offering potential insights into its pathogenesis and therapeutic strategies.

**Supplementary Materials:** The following supporting information can be downloaded at: <https://media.sciltp.com/articles/others/2507031521511272/HM-770-SI-FC-done.pdf>.

**Author Contributions:** Y.R.: Conceptualization, Investigation, Methodology, Data Curation, Writing—Original Draft Preparation; L.X.: Conceptualization, Data Curation, Methodology; Q.S.: Data Curation, Methodology; X.S.: Methodology; A.X.: Supervision, Validation; Z.C.: Supervision, Validation, Writing—Review and Editing. All authors have read and agreed to the published version of the manuscript.

**Funding:** This work was supported by the Hong Kong Research Grants Council Area of Excellence (AoE/M/707-18) and the National Natural Science Foundation of China (22036001, 82161138026 and 82070860).

**Institutional Review Board Statement:** The study was conducted according to the guidelines of the Chinese University of Hong Kong (CUHK), and approved by the Hong Kong Government and Department of Health.

**Informed Consent Statement:** Not applicable.

**Data Availability Statement:** Not applicable.

**Conflicts of Interest:** The authors declare that they have no known competing financial interests or personal relationships that could have appeared to influence the work reported in this paper.

## References

1. Shang, Y.; Grip, E.T.; Modica, A.; Skróder, H.; Ström, O.; Ntanos, F.; Gudbjörnsdóttir, S.; Hagström, H. Metabolic syndrome traits increase the risk of major adverse liver outcomes in type 2 diabetes. *Diabetes Care* **2024**, *47*, 978–985.
2. Chandrasekaran, P.; Weiskirchen, R. Cellular and molecular mechanisms of insulin resistance. *Curr. Tissue Microenviron. Rep.* **2024**, *5*, 79–90.
3. Mallick, R.; Basak, S.; Das, R.K.; Banerjee, A.; Paul, S.; Pathak, S.; Duttaroy, A.K. Fatty acids and their proteins in adipose tissue inflammation. *Cell Biochem. Biophys.* **2024**, *82*, 35–51.
4. Sancar, G.; Birkenfeld, A.L. The role of adipose tissue dysfunction in hepatic insulin resistance and T2D. *J. Endocrinol.* **2024**, *262*, e240115.
5. Unamuno, X.; Gómez-Ambrosi, J.; Rodríguez, A.; Becerril, S.; Frühbeck, G.; Catalán, V. Adipokine dysregulation and adipose tissue inflammation in human obesity. *Eur. J. Clin. Investig.* **2018**, *48*, e12997.
6. Itoh, N. FGF21 as a hepatokine, adipokine, and myokine in metabolism and diseases. *Front. Endocrinol.* **2014**, *5*, 107.
7. Kojta, I.; Chacińska, M.; Błachnio-Zabielska, A. Obesity, bioactive lipids, and adipose tissue inflammation in insulin resistance. *Nutrients* **2020**, *12*, 1305.
8. Mathioudaki, A.; Fanni, G.; Eriksson, J.W.; Pereira, M.J. Metabolomic Profiling of Adipose Tissue in Type 2 Diabetes: Associations with Obesity and Insulin Resistance. *Metabolites* **2024**, *14*, 411.
9. Xiang, L.; Wang, L.; Xia, Y.; Wang, Y.; Shi, J.; Zhang, C.-L.; Xie, L.; Ru, Y.; Cheng, C.K.; Pu, Y. Exercise alleviates

- diabetic kidney disease through PPAR $\delta$ -CPT1 $\alpha$  pathway-dependent fatty acid  $\beta$ -oxidation. *Innov. Life* **2024**, *2*, 100065.
10. Wang, S.; He, T.; Wang, H. Non-targeted metabolomics study for discovery of hepatocellular carcinoma serum diagnostic biomarker. *J. Pharm. Biomed. Anal.* **2024**, *239*, 115869.
  11. Chen, Y.; Wang, B.; Zhao, Y.; Shao, X.; Wang, M.; Ma, F.; Yang, L.; Nie, M.; Jin, P.; Yao, K. Metabolomic machine learning predictor for diagnosis and prognosis of gastric cancer. *Nat. Commun.* **2024**, *15*, 1657.
  12. Giesbertz, P.; Padberg, I.; Rein, D.; Ecker, J.; Höfle, A.S.; Spanier, B.; Daniel, H. Metabolite profiling in plasma and tissues of ob/ob and db/db mice identifies novel markers of obesity and type 2 diabetes. *Diabetologia* **2015**, *58*, 2133–2143.
  13. Xiang, L.; Wei, J.; Tian, X.Y.; Wang, B.; Chan, W.; Li, S.; Tang, Z.; Zhang, H.; Cheang, W.S.; Zhao, Q. Comprehensive analysis of acylcarnitine species in db/db mouse using a novel method of high-resolution parallel reaction monitoring reveals widespread metabolic dysfunction induced by diabetes. *Anal. Chem.* **2017**, *89*, 10368–10375.
  14. Xiang, L.; Ru, Y.; Shi, J.; Wang, L.; Zhao, H.; Huang, Y.; Cai, Z. Derivatization of N-Acyl Glycines by 3-Nitrophenylhydrazine for Targeted Metabolomics Analysis and Their Application to the Study of Diabetes Progression in Mice. *Anal. Chem.* **2023**, *95*, 2183–2191.
  15. Mora-Ortiz, M.; Nunez Ramos, P.; Oregioni, A.; Claus, S.P. NMR metabolomics identifies over 60 biomarkers associated with Type II Diabetes impairment in db/db mice. *Metabolomics* **2019**, *15*, 89.
  16. Ribbenstedt, A.; Ziarrusta, H.; Benskin, J.P. Development, characterization and comparisons of targeted and non-targeted metabolomics methods. *PLoS ONE* **2018**, *13*, e0207082.
  17. Zhang, X.; Zhu, X.; Wang, C.; Zhang, H.; Cai, Z. Non-targeted and targeted metabolomics approaches to diagnosing lung cancer and predicting patient prognosis. *Oncotarget* **2016**, *7*, 63437.
  18. Wang, R.; Li, B.; Lam, S.M.; Shui, G. Integration of lipidomics and metabolomics for in-depth understanding of cellular mechanism and disease progression. *J. Genet. Genom.* **2020**, *47*, 69–83.
  19. Chen, Z.; Liang, Q.; Wu, Y.; Gao, Z.; Kobayashi, S.; Patel, J.; Li, C.; Cai, F.; Zhang, Y.; Liang, C. Comprehensive lipidomic profiling in serum and multiple tissues from a mouse model of diabetes. *Metabolomics* **2020**, *16*, 115.
  20. Jin, L.; Shi, F.; Chun, Q.; Chen, H.; Ma, Y.; Wu, S.; Hameed, N.F.; Mei, C.; Lu, J.; Zhang, J. Artificial intelligence neuropathologist for glioma classification using deep learning on hematoxylin and eosin stained slide images and molecular markers. *Neuro-oncology* **2021**, *23*, 44–52.
  21. Xiang, L.; Nie, J.; Wang, L.; Wang, Y.; Shi, J.; Wei, J.; Lau, C.-W.; Cai, Z.; Huang, Y. Integrated metabolomics analysis of the effect of PPAR $\delta$  agonist GW501516 on catabolism of BCAAs and carboxylic acids in diabetic mice. *Chin. Chem. Lett.* **2021**, *32*, 2197–2202.
  22. Xie, G.; Wang, L.; Chen, T.; Zhou, K.; Zhang, Z.; Li, J.; Sun, B.; Guo, Y.; Wang, X.; Wang, Y. A metabolite array technology for precision medicine. *Anal. Chem.* **2021**, *93*, 5709–5717.
  23. Papandreou, C.; Li, J.; Liang, L.; Bulló, M.; Zheng, Y.; Ruiz-Canela, M.; Yu, E.; Guasch-Ferré, M.; Razquin, C.; Clish, C. Metabolites related to purine catabolism and risk of type 2 diabetes incidence; modifying effects of the TCF7L2-rs7903146 polymorphism. *Sci. Rep.* **2019**, *9*, 2892.
  24. Xia, J.; Wang, Z.; Zhang, F. Association between related purine metabolites and diabetic retinopathy in type 2 diabetic patients. *Int. J. Endocrinol.* **2014**, *2014*, 651050.
  25. Varadaiah, Y.G.C.; Sivanesan, S.; Nayak, S.B.; Thirumalarao, K.R. Purine metabolites can indicate diabetes progression. *Arch. Physiol. Biochem.* **2022**, *128*, 87–91.
  26. Romeo, G.R.; Jain, M. Purine metabolite signatures and type 2 Diabetes: Innocent bystanders or actionable items? *Curr. Diabetes Rep.* **2020**, *20*, 30.
  27. Cole, J.B.; Florez, J.C. Genetics of diabetes mellitus and diabetes complications. *Nat. Rev. Nephrol.* **2020**, *16*, 377–390.
  28. Mabley, J.G.; Pacher, P.; Liaudet, L.; Soriano, F.G.; Hasko, G.; Marton, A.; Szabo, C.; Salzman, A.L. Inosine reduces inflammation and improves survival in a murine model of colitis. *Am. J. Physiol.-Gastrointest. Liver Physiol.* **2003**, *284*, G138–G144.
  29. Sautin, Y.Y.; Johnson, R.J. Uric acid: The oxidant-antioxidant paradox. *Nucleosides Nucleotides Nucleic Acids* **2008**, *27*, 608–619.
  30. Ruhál, P.; Dhingra, D. Inosine improves cognitive function and decreases aging-induced oxidative stress and neuroinflammation in aged female rats. *Inflammopharmacology* **2018**, *26*, 1317–1329.
  31. Gualano, B.; Everaert, I.; Stegen, S.; Artioli, G.G.; Taes, Y.; Roschel, H.; Achten, E.; Otaduy, M.C.; Junior, A.H.L.; Harris, R. Reduced muscle carnosine content in type 2, but not in type 1 diabetic patients. *Amino Acids* **2012**, *43*, 21–24.
  32. Peters, V.; Lanthaler, B.; Amberger, A.; Fleming, T.; Forsberg, E.; Hecker, M.; Wagner, A.H.; Yue, W.W.; Hoffmann, G.F.; Nawroth, P. Carnosine metabolism in diabetes is altered by reactive metabolites. *Amino Acids* **2015**, *47*, 2367–2376.
  33. Zhou, Y.; Zhao, R.; Lyu, Y.; Shi, H.; Ye, W.; Tan, Y.; Li, R.; Xu, Y. Serum and amniotic fluid metabolic profile changes in response to gestational diabetes mellitus and the association with maternal–fetal outcomes. *Nutrients* **2021**, *13*, 3644.
  34. Hrubisko, M.; Danis, R.; Huorka, M.; Wawruch, M. Histamine intolerance—The more we know the less we know. A review. *Nutrients* **2021**, *13*, 2228.

35. Hussein, M.M.; Zakaria, G.; Abdelkhalek, A.; Arisha, A.H. Histidine-Containing Dipeptide and Diabetic Complications. *J. Adv. Vet. Res.* **2023**, *13*, 685–692.
36. Cesak, O.; Vostalova, J.; Vidlar, A.; Bastlova, P.; Student Jr, V. Carnosine and beta-alanine supplementation in human medicine: Narrative review and critical assessment. *Nutrients* **2023**, *15*, 1770.
37. Yousri, N.A.; Suhre, K.; Yassin, E.; Al-Shakaki, A.; Robay, A.; Elshafei, M.; Chidiac, O.; Hunt, S.C.; Crystal, R.G.; Fakhro, K.A. Metabolic and metabo-clinical signatures of type 2 diabetes, obesity, retinopathy, and dyslipidemia. *Diabetes* **2022**, *71*, 184–205.
38. Nilsen, M.S.; Jersin, R.Å.; Ulvik, A.; Madsen, A.; McCann, A.; Svensson, P.-A.; Svensson, M.K.; Nedrebø, B.G.; Gudbrandsen, O.A.; Tell, G.S. 3-Hydroxyisobutyrate, a strong marker of insulin resistance in type 2 diabetes and obesity that modulates white and brown adipocyte metabolism. *Diabetes* **2020**, *69*, 1903–1916.
39. Mihalik, S.J.; Michaliszyn, S.F.; De Las Heras, J.; Bacha, F.; Lee, S.; Chace, D.H.; DeJesus, V.R.; Vockley, J.; Arslanian, S.A. Metabolomic profiling of fatty acid and amino acid metabolism in youth with obesity and type 2 diabetes: Evidence for enhanced mitochondrial oxidation. *Diabetes Care* **2012**, *35*, 605–611.
40. Weiser, A.; Giesbertz, P.; Daniel, H.; Spanier, B. Acylcarnitine profiles in plasma and tissues of hyperglycemic NZO mice correlate with metabolite changes of human diabetes. *J. Diabetes Res.* **2018**, *2018*, 1864865.
41. Batchuluun, B.; Al Rijjal, D.; Prentice, K.J.; Eversley, J.A.; Burdett, E.; Mohan, H.; Bhattacharjee, A.; Gunderson, E.P.; Liu, Y.; Wheeler, M.B. Elevated medium-chain acylcarnitines are associated with gestational diabetes mellitus and early progression to type 2 diabetes and induce pancreatic  $\beta$ -cell dysfunction. *Diabetes* **2018**, *67*, 885–897.
42. Li, M.; Wang, X.; Aa, J.; Qin, W.; Zha, W.; Ge, Y.; Liu, L.; Zheng, T.; Cao, B.; Shi, J. GC/TOFMS analysis of metabolites in serum and urine reveals metabolic perturbation of TCA cycle in db/db mice involved in diabetic nephropathy. *Am. J. Physiol.-Ren. Physiol.* **2013**, *304*, F1317–F1324.
43. Hoene, M.; Kappler, L.; Kollipara, L.; Hu, C.; Irmeler, M.; Bleher, D.; Hoffmann, C.; Beckers, J.; de Angelis, M.H.; Häring, H.-U. Exercise prevents fatty liver by modifying the compensatory response of mitochondrial metabolism to excess substrate availability. *Mol. Metab.* **2021**, *54*, 101359.
44. Houten, S.M.; Wanders, R.J. A general introduction to the biochemistry of mitochondrial fatty acid  $\beta$ -oxidation. *J. Inherit. Metab. Dis.* **2010**, *33*, 469–477.
45. Lu, J.; Lam, S.M.; Wan, Q.; Shi, L.; Huo, Y.; Chen, L.; Tang, X.; Li, B.; Wu, X.; Peng, K. High-coverage targeted lipidomics reveals novel serum lipid predictors and lipid pathway dysregulation antecedent to type 2 diabetes onset in normoglycemic Chinese adults. *Diabetes Care* **2019**, *42*, 2117–2126.
46. Summers, S.A. Ceramides in insulin resistance and lipotoxicity. *Prog. Lipid Res.* **2006**, *45*, 42–72.
47. Raichur, S.; Brunner, B.; Bielohuby, M.; Hansen, G.; Pfenninger, A.; Wang, B.; Bruning, J.C.; Larsen, P.J.; Tennagels, N. The role of C16: 0 ceramide in the development of obesity and type 2 diabetes: CerS6 inhibition as a novel therapeutic approach. *Mol. Metab.* **2019**, *21*, 36–50.
48. Montgomery, M.K.; Brown, S.H.; Lim, X.Y.; Fiveash, C.E.; Osborne, B.; Bentley, N.L.; Braude, J.P.; Mitchell, T.W.; Coster, A.C.; Don, A.S. Regulation of glucose homeostasis and insulin action by ceramide acyl-chain length: A beneficial role for very long-chain sphingolipid species. *Biochim. Et Biophys. Acta (BBA)-Mol. Cell Biol. Lipids* **2016**, *1861*, 1828–1839.
49. Mandal, N.; Grambergs, R.; Mondal, K.; Basu, S.K.; Tahia, F.; Dagogo-Jack, S. Role of ceramides in the pathogenesis of diabetes mellitus and its complications. *J. Diabetes Its Complicat.* **2021**, *35*, 107734.
50. Düsing, P.; Heinrich, N.N.; Al-Kassou, B.; Gutbrod, K.; Dörmann, P.; Nickenig, G.; Jansen, F.; Zietzer, A. Analysis of circulating ceramides and hexosylceramides in patients with coronary artery disease and type II diabetes mellitus. *BMC Cardiovasc. Disord.* **2023**, *23*, 454.
51. Sokołowska, E.; Car, H.; Fiedorowicz, A.; Szelachowska, M.; Milewska, A.; Wawrusiewicz-Kurylonek, N.; Szumowski, P.; Krzyżanowska-Grycel, E.; Popławska-Kita, A.; Żendzian-Piotrowska, M. Sphingomyelin profiling in patients with diabetes could be potentially useful as differential diagnostics biomarker: A pilot study. *Adv. Med. Sci.* **2022**, *67*, 250–256.
52. Qian, X.; Jia, H.; Wang, J.; He, S.; Yu, M.; Feng, X.; Gong, Q.; An, Y.; Wang, X.; Shi, N. Circulating palmitoyl sphingomyelin levels predict the 10-year increased risk of cardiovascular disease death in Chinese adults: Findings from the Da Qing Diabetes Study. *Cardiovasc. Diabetol.* **2024**, *23*, 37.
53. Shao, F.; Hu, X.; Li, J.; Bai, B.; Tian, L. Lipidomics analysis of impaired glucose tolerance and type 2 diabetes mellitus in overweight or obese elderly adults. *Endocr. Connect.* **2023**, *12*, e230212.
54. Yang, Q.; Vijayakumar, A.; Kahn, B.B. Metabolites as regulators of insulin sensitivity and metabolism. *Nat. Rev. Mol. Cell Biol.* **2018**, *19*, 654–672.
55. Xu, H.; Li, W.; Huang, L.; He, X.; Xu, B.; He, X.; Chen, W.; Wang, Y.; Xu, W.; Wang, S. Phosphoethanolamine cytidyltransferase ameliorates mitochondrial function and apoptosis in hepatocytes in T2DM in vitro. *J. Lipid Res.* **2023**, *64*, 100337.